SCIENCE CHINA
Chemistry

• ARTICLES •

September 2012 Vol.55 No.9: 1802–1810
doi: 10.1007/s11426-012-4721-8

Preparation, characterization and photocatalytic performance of Mo-doped ZnO photocatalysts

YU ChangLin[1*], YANG Kai[1,2], SHU Qing[1], YU Jimmy C.[3], CAO FangFang[1], LI Xin[1] & ZHOU XiaoChun[1]

[1]*School of Metallurgy and Chemical Engineering, Jiangxi University of Science and Technology, Ganzhou 341000, China*
[2]*Fujian Provincial Key Laboratory of Photocatalysis—State Key Laboratory Breeding Base, Fuzhou University, Fuzhou 350002, China*
[3]*Department of Chemistry, The Center of Novel Functional Molecules and Environmental Science Programme, The Chinese University of Hong Kong, Shatin, New Territories, Hong Kong, China*

Received April 24, 2011; accepted December 9, 2011; published online August 7, 2012

A series of Mo-doped ZnO photocatalysts with different Mo-dopant concentrations have been prepared by a grinding–calcination method. The structure of these photocatalysts was characterized by a variety of methods, including N_2 physical adsorption, X-ray diffraction (XRD), scanning electron microscopy (SEM), Fourier transform infrared (FT-IR) spectroscopy, photoluminescence (PL) emission spectroscopy, and UV-vis diffuse reflectance spectroscopy (DRS). It was found that Mo^{6+} could enter into the crystal lattice of ZnO due to the radius of Mo^{6+} (0.065 nm) being smaller than that of Zn^{2+} (0.083 nm). XRD results indicated that Mo^{6+} suppressed the growth of ZnO crystals. The FT-IR spectroscopy results showed that the ZnO with 2 wt.% Mo-doping has a higher level of surface hydroxyl groups than pure ZnO. PL spectroscopy indicated that ZnO with 2 wt.% Mo-doping also exhibited the largest reduction in the intensity of the emission peak at 390 nm caused by the recombination of photogenerated hole-electron pairs. The activities of the Mo-doped ZnO photocatalysts were investigated in the photocatalytic degradation of acid orange II under UV light (λ = 365 nm) irradiation. It was found that ZnO with 2 wt.% Mo-doping showed much higher photocatalytic activity and stability than pure ZnO. The high photocatalytic performance of the Mo-doped ZnO can be attributed to a great improvement in the surface properties of ZnO, higher crystallinity and lower recombination rate of photogenerated hole-electron (e^-/h^+) pairs. Moreover, the undoped Mo species may exist in the form of MoO_3 and form MoO_3/ZnO heterojunctions which further favors the separation of e^-/h^+ pairs.

ZnO, Mo doping, e^-/h^+ pairs, photocatalysis, acid orange II

1 Introduction

Recently, semiconductor photocatalysis based on the utilization of solar energy has attracted a lot of attention due to its promising applications like water disinfection, and the degradation and complete mineralization of organic contaminants in waste water [1–7]. Zinc oxide, a semiconductor with a large excitation energy [8] of 60 meV, plays an important role in many application fields, such as optoelectronics, photocatalysis, and gas sensing [9–12]. However, as a photocatalyst, ZnO shows a low activity compared with commercial TiO_2 catalysts in the photocatalytic degradation of organic compounds. Moreover, ZnO suffers from photoinstability in aqueous solution due to its problem of photocorrosion. Thus, improving both the activity and stability is important if ZnO is to be employed as an effective photocatalyst. Several methods have been reported to improve the photocatalytic performance of ZnO, such as noble metal deposition [13, 14], semiconductor coupling [15, 16], nonmetal element doping [17, 18], and polymer composite formation [19, 20]. Kislov *et al.* [21] investigated the photo-

*Corresponding author (email: yuchanglinjx@163.com)

stability and photocatalytic activity of different crystal surfaces of ZnO. They found that photostability and photocatalytic activity were strongly dependent on its surface atomic structures. If the surface is polar and has high surface energy, photolysis of ZnO easily takes place, which causes the problem of photocorrosion. Shen *et al.* [22] reported that doping of transition metals (Cr, Mn, Fe, Co, Ni, Cu) could induce a change in the cohesive energy, density of states, band structure, and optical absorption properties of ZnO. Our recent research has shown that doping of Ce into ZnO causes an increase in surface hydroxyl groups and suppresses the recombination rate of electron/hole (e^-/h^+) pairs [23]. Inspired by these investigations, in this work, we fabricated a series of Mo-doped ZnO photocatalysts with different Mo concentrations and investigated the influences of Mo doping on the structure and photocatalytic performance of ZnO.

2 Experimental

2.1 Synthesis

All chemicals were of analytical grade and used as received without further purification. In a typical synthesis, 0.1 g of hexadecyltrimethylammonium bromide (CTAB) surfactant (AR, Sinopharm Chemical Reagent Co. Ltd.), 50 mL of deionized (DI) water and 3.673 g of $Zn(NO_3)_2{\cdot}6H_2O$ (AR, Sinopharm Chemical Reagent Co. Ltd.) were mixed, to give solution A; 0.988 g of NaOH (AR, Sinopharm Chemical Reagent Co. Ltd.) and 50 mL of DI water were mixed, to give solution B. Solution B was added dropwise to solution A with magnetic stirring and the final mixture further stirred for half an hour. The resulting precipitate was centrifuged and washed with DI water and absolute ethanol in sequence, and finally dried at 80 °C in an oven for 12 h to obtain $Zn(OH)_2$. According to the required doping concentration, a certain amount of $(NH_4)_6Mo_7O_{24}{\cdot}4H_2O$ (AR, Sinopharm Chemical Reagent Co. Ltd.) was mixed with the $Zn(OH)_2$ and the mixture was ground for 1 h. The mixture was then heated in air at a ramp rate of 3 °C/min to 600 °C and calcined for 2 h, and finally naturally cooled to room temperature. The final Mo content in ZnO was determined by X-ray fluorescence analysis (Magix 601). The photocatalysts are denoted Mo(1%)/ZnO, Mo(2%)/ZnO, Mo(3%)/ZnO and Mo(8%)/ZnO indicating the wt.% amount of Mo in the photocatalyst.

2.2 Characterization

The Brunauer–Emmett–Teller (BET) surface areas of the sample were obtained from N_2 adsorption/desorption isotherms on an automatic analyzer (NOVA 4000). The samples were outgassed for 2 h under vacuum at 350 °C prior to adsorption. Powder X-ray diffraction data (XRD) were recorded at a scanning rate of 0.01° s^{-1} using a Bruker D8 ADVANCE X-ray diffractometer at 40 kV and 40 mA with monochromatized Cu Kα (λ = 1.54178 nm) radiation. Scanning electron microscopy (SEM) measurements were carried out on a XL30 (Philips, the Netherlands) scanning electron microscope, which was used to investigate the morphology and surface roughness of samples. The products were conductively coated with gold by sputtering for 30 s to minimize charging effects before SEM imaging was performed. Fourier transform infrared (FT-IR) spectra were recorded with a Nicolet 470 FTIR spectrometer (USA) with a resolution of 4 cm^{-1}. Samples were pressed into KBr disks. The samples were dried at 250 °C for 2 h before pressing. To investigate the recombination and lifespan of photogenerated e^-/h^+ pairs in the photocatalysts, the photoluminescence (PL) emission spectra of the samples were recorded. A 320 nm He–Cd laser was used as an excitation light source. The emission from the sample was measured by a spectrometer (Spex 500M, USA) equipped with a photon counter (SR400, USA). UV–vis diffuse reflectance spectra (DRS) were measured using a UV–vis spectrophotometer (UV-2550, Shimadzu). Absorption spectra were referenced to $BaSO_4$.

2.3 Photocatalytic activity measurements

The photocatalytic activities of the samples were determined by measuring the degradation of acid orange II in an aqueous solution under ultraviolet light irradiation. In activity tests, a 365 nm UV lamp (15 W, Cole-Parmer Instrument Co.) was used as ultraviolet light source. The photocatalyst (0.05 g) was suspended in 80 mL of aqueous solution of acid orange II with a concentration of C_0 = 0.020 g/L. Prior to light illumination, the suspension was strongly magnetically stirred for 40 min in the dark to establish adsorption /desorption equilibrium. The suspension was vigorously stirred in the photoreactor during the process and the temperature of the suspension was maintained at 22 ± 2 °C by circulation of water through an external cooling coil. At given intervals of illumination, aliquots of the suspension were removed and centrifuged. The clear upper layer solution was analyzed using a spectrophotometer (UV-2550, Shimadzu). The dye concentration was measured at λ = 478 nm, which is the maximum absorption wavelength for acid orange II. The degradation ratio (D) of acid orange II was calculated according to the equation:

$$D = (C_0 - C)/C_0 \times 100\%$$

where C_0 is the initial absorbance and C is the final absorbance.

3 Results and discussion

3.1 XRD analysis

XRD was used to investigate the crystalline nature of the prepared samples. The XRD patterns for the pure ZnO and

Mo-doped ZnO samples are shown in Figure 1(a). Clear characteristic peaks at 2θ values of 32.0, 34.6, 36.4, 47.8, 56.9, 63.0, 66.5, 68.1 and 69.2° are observed, and can be indexed to the standard card for hexagonal wurtzite ZnO (JCPDS No.36-1451). The sharp diffraction peaks demonstrate that these samples have high crystallinity. Moreover, no characteristic peaks of impurities, such as MoO_3 and $Zn(OH)_2$, were detected in the diffraction patterns of the composite samples, confirming that $Zn(OH)_2$ was converted to ZnO, and that Mo exists in a highly dispersed state. Figure 1(b) shows XRD patterns of Mo(2%)ZnO calcined at different temperatures. No changes in the position of the diffraction peaks were observed, which indicates that no new crystalline phases were produced. With increasing calcination temperature, the intensity of the diffraction peaks of ZnO gradually increases, indicating an improvement in crystallinity.

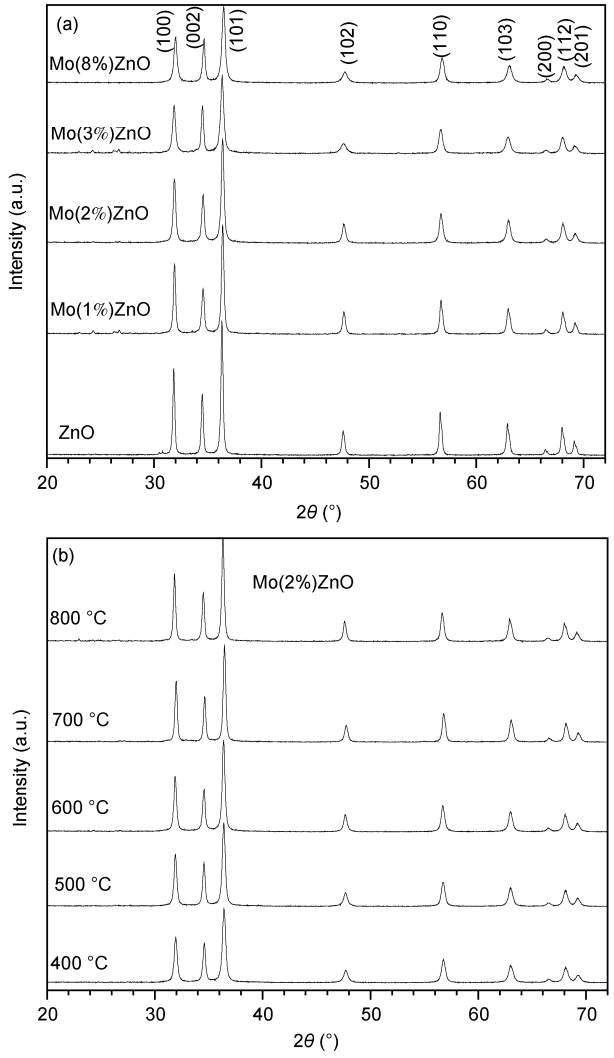

Figure 1 X-ray diffraction patterns of the samples. (a) Zinc oxide and Mo-doped ZnO with different Mo contents calcined at 600 °C; (b) Mo(2%)ZnO calcined at different temperatures.

The average crystallite sizes of all samples were estimated according to the Scherrer equation [24, 25]: $D = 0.89\lambda/(\beta\cos\theta)$, where β is the width in radians of the XRD peak at half the peak height for the (101) reflection, λ is the wavelength of the X-rays in nanometers (λ = 0.154178 nm), θ is the angle between the incident and diffracted beams in degrees, and D is the average crystallite size of the powder sample in nanometers. The calculated average crystallite sizes are summarized in Table 1. It can be seen that both Mo-doping and calcination temperature have an influence on the average grain size of the sample. The presence of Mo apparently restrains the growth of ZnO crystallites. A possible reason for the decrease in ZnO crystallite size could be that some Mo^{6+} entered into the crystal lattice of ZnO and suppressed the growth of the ZnO crystal, because the radius of Mo^{6+} (0.065 nm) is smaller than that of Zn^{2+} (0.083 nm). However, increasing the calcination temperature causes an increase in grain size, which may be mainly due to the sintering of small ZnO particles at high calcination temperatures.

3.2 Microstructure analysis

The morphology of the synthesized samples was analyzed by SEM. Figure 2 shows the typical SEM images of the pure ZnO and Mo-doped ZnO photocatalysts. Figures 2(a)–(c) show that at the same calcination temperature, no significant differences in morphology can be observed between the pure ZnO and ZnO with different Mo-doping concentrations. All samples are composed of a large number of loose and dispersed small particles. Figures 2(d) and (e) show the effect of varying the calcination temperature on the microstructure of the Mo(2%)ZnO. It can be seen that when the sample was calcined at 800 °C, very big particles appeared and the sample showed a poor dispersion which is caused by the sintering of small particles at such an elevated temperature. The microstructures of the prepared samples were further analyzed by N_2 adsorption. The BET surface area of the samples is summarized in Table 2. It can be seen that the specific surface area of the Mo-doped ZnO sample increases slightly with increasing Mo doping content, which

Table 1 Average grain size of the zinc oxide samples with different Mo contents and Mo(2%)ZnO samples calcined at different temperatures

Sample	Calcination temperature (°C)	D (nm)
ZnO	600	34.26
Mo(1%)ZnO	600	29.23
Mo(2%)ZnO	600	27.57
Mo(3%)ZnO	600	23.82
Mo(8%)ZnO	600	22.68
Mo(2%)ZnO	400	22.09
Mo(2%)ZnO	500	22.52
Mo(2%)ZnO	700	29.56
Mo(2%)ZnO	800	30.12

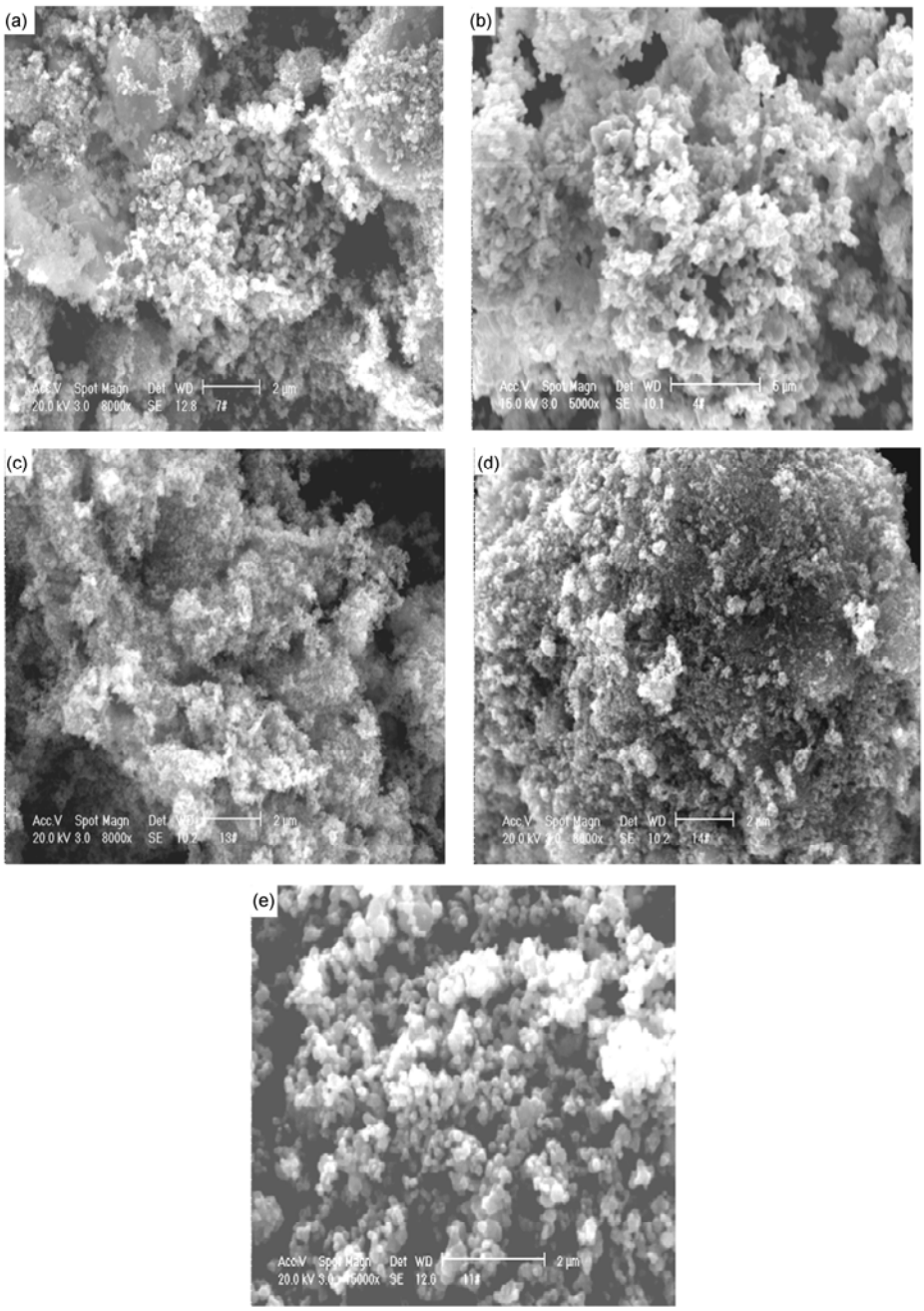

Figure 2 SEM images of the samples. (a) ZnO calcined at 600 °C; (b) Mo(2%)ZnO calcined at 600 °C; (c) Mo(8%)ZnO calcined at 600 °C; (d) Mo(2%)ZnO calcined at 400 °C; (e) Mo(2%)ZnO calcined at 800 °C.

is possibly caused by the decrease in crystallite size of ZnO due to the presence of Mo. An increase in specific surface area can favor the adsorption of a dye and increase the photocatalytic activity of ZnO [26]. Moreover, increasing the calcination temperature results in a decrease in surface area. This can be attributed to sintering of the ZnO particles, in agreement with the XRD and SEM data.

3.3 FT-IR analysis

The FT-IR spectra of the samples are shown in Figure 3. All the samples have a peak at around 3440 cm^{-1} which can be assigned to the stretching vibration and bending vibration of surface hydroxyl groups on ZnO. From Figure 3(a), it can be seen that the intensity of the absorption peak of –OH groups markedly increases after Mo doping and the intensity of this peak reaches a maximum for ZnO with 2 wt.% Mo. In photocatalytic reactions, the activity is closely related to the number of –OH groups on the catalyst because the –OH groups can capture the photogenerated holes (h^+) and transform to an $^{\bullet}OH$ radical which is the main reactive species

Table 2 Specific surface areas of the zinc oxide samples with different Mo contents and Mo(2%)ZnO samples calcined at different temperatures

Sample	Calcination temperature (°C)	Surface area (m^2/g)
ZnO	600	12.06
Mo(1%)ZnO	600	12.13
Mo(2%)ZnO	600	14.08
Mo(3%)ZnO	600	14.56
Mo(8%)ZnO	600	15.42
Mo(2%)ZnO	400	18.03
Mo(2%)ZnO	500	16.67
Mo(2%)ZnO	700	7.03
Mo(2%)ZnO	800	5.28

for the decomposition of dyes [27]. Therefore, an increase in the number of –OH groups can improve the photocatalytic activity. The peak at 1630 cm^{-1} is assigned to the bending vibration of adsorbed water on the surface of the catalyst. The peak at around 440 cm^{-1} is attributed to the stretching vibration of Zn–O bonds. It has been reported in ref. [28] that five characteristic peaks for MoO_3 occur at around 553, 876, 995, 1630 and 3445 cm^{-1}, respectively. However, no such peaks for MoO_3 are observed for any of the doped samples. A possible reason is that a strong interaction between MoO_3 and ZnO may occur and the interaction could cause the disappearance of the characteristic peaks of MoO_3. Two peaks at around 1388 and 1124 cm^{-1} could be ascribed to the formation of a Mo–O–Zn bond because these two peaks were not found for either MoO_3 and ZnO. Figure 3(b) shows that, at the same concentration of Mo, with the increase of calcination temperature from 400 to 600 °C, the intensity of the peak at around 1124 cm^{-1} increases gradually, which indicates that in this temperature range, an increase in calcination temperature strengthens the interactions between MoO_3 and ZnO and more Mo–O–Zn bonds are produced. However, when the calcination temperature was increased to 700 or 800 °C, the intensity of this peak began to decrease. The high calcination temperatures also decreased the intensity of the peak at around 3440 cm^{-1} because treatment at elevated temperature causes the loss of –OH groups and a decrease in the specific surface area.

3.4 UV–vis diffuse reflectance spectra

Figure 4 shows the UV–vis diffuse reflectance spectra of pristine and Mo-doped ZnO catalysts. From this figure, it can be seen that Mo doping has a slight influence on the absorption edge of zinc oxide. The band gap energy (E_g) for the catalyst was determined using the equation $E_g = 1240/\lambda_g$ (eV), where λ_g is the absorption edge which was obtained from the intercept between the tangent of the absorption curve and the abscissa. The calculated band gap energies for different samples are shown in Table 3. Figure 4(a) shows that pure ZnO has strong UV light absorption from 300 to 380 nm and very weak absorption in the visible light range.

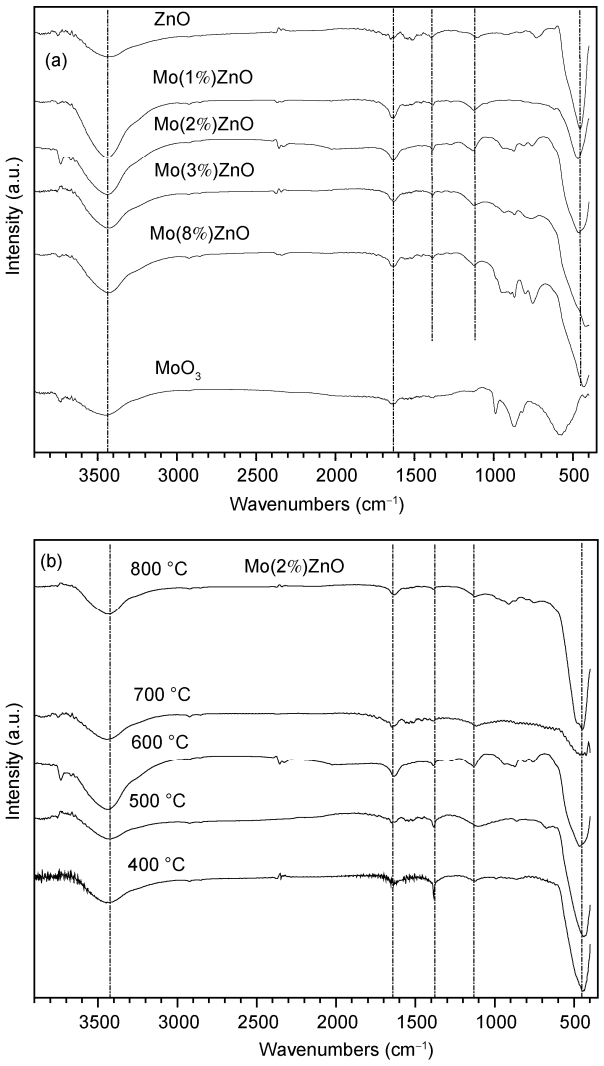

Figure 3 FT-IR infrared spectra of the samples. (a) Samples with different Mo contents calcined at 600 °C; (b) Mo(2%)ZnO calcined at different temperatures.

Doping with Mo causes the absorption edge of ZnO to shift slightly in the long wavelength direction and thus decreases the band gap energy. Figure 4(b) indicates that the calcination temperature has relatively little influence on the light absorption of the Mo(2%)ZnO.

Table 3 Band gap energies of the samples

Sample	Calcination temperature (°C)	E_g (eV)
ZnO	600	3.20
Mo(1%)ZnO	600	3.10
Mo(2%)ZnO	600	3.09
Mo(3%)ZnO	600	3.09
Mo(8%)ZnO	600	3.08
Mo(2%)ZnO	400	3.11
Mo(2%)ZnO	500	3.08
Mo(2%)ZnO	700	3.13
Mo(2%)ZnO	800	3.14
MoO_3	600	2.87

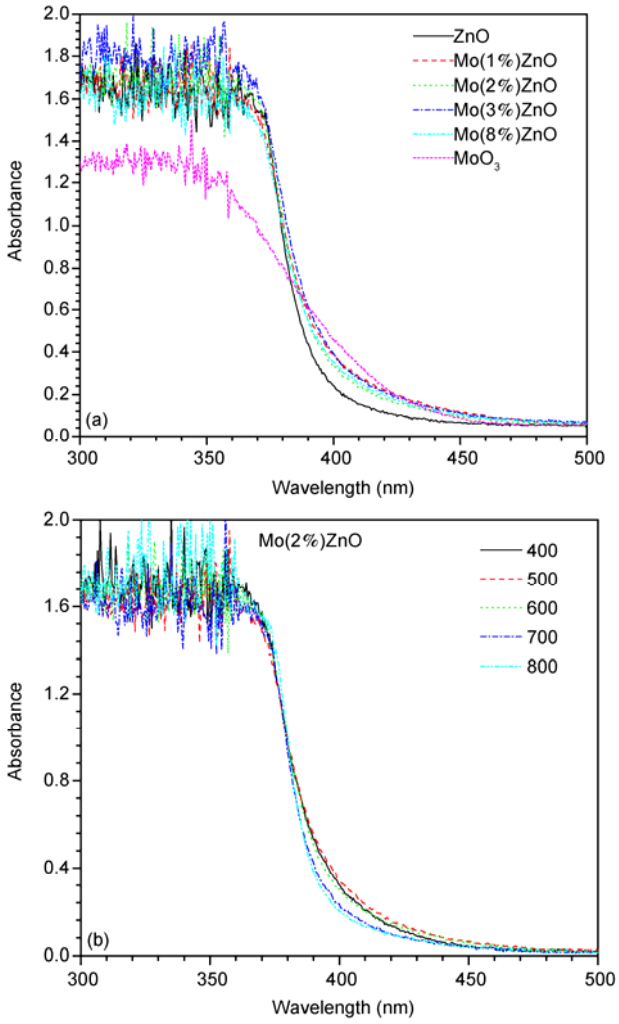

Figure 4 UV–vis spectra of the samples. (a) Samples with different Mo contents calcined at 600 °C; (b) Mo(2%)ZnO calcined at different temperatures.

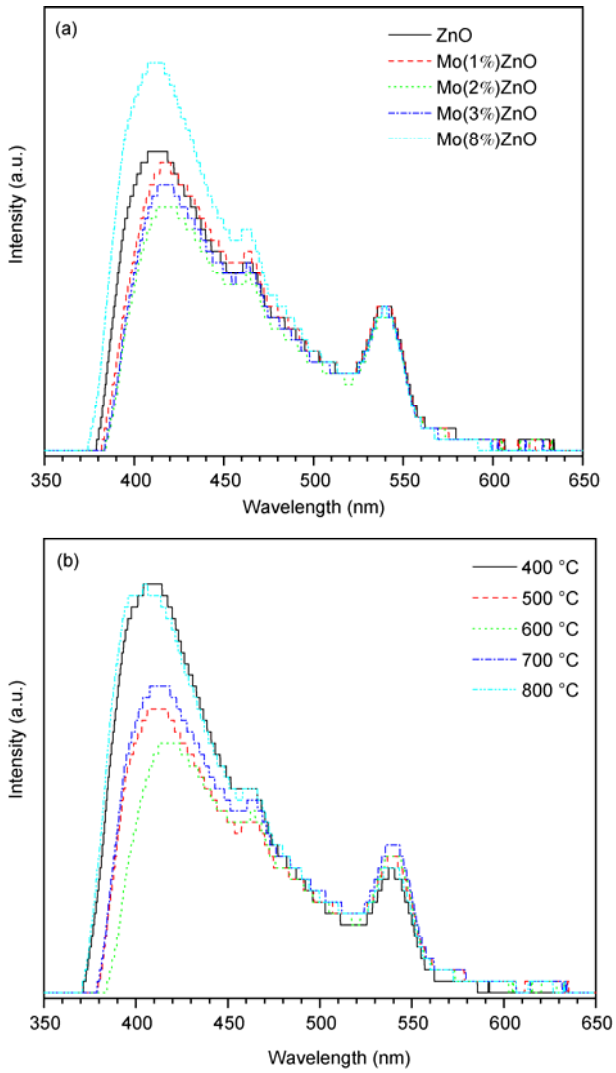

Figure 5 Photoluminescence spectra of the samples. (a) Samples with different Mo contents calcined at 600 °C; (b) Mo(2%)ZnO calcined at different temperatures.

3.5 PL emission spectra

To investigate the charge carrier trapping, immigration and transfer, as well as to understand the fate of photogenerated electron and hole pairs in semiconductor particles, the PL emission spectra of the pure ZnO and Mo-doped ZnO samples were recorded at room temperature as shown in Figure 5. All samples show three obvious characteristic emission peaks at around 390, 460 and 540 nm in the PL spectra. The emission peak at 390 nm near the ultraviolet range is due to the recombination of photogenerated electrons and holes [29, 30]. There is some controversy in the reference about the origins of the other two emission peaks in the range 420–620 nm. One explanation [31] is that this emission is an indirect emission which is related to surface vacancies on ZnO. Figure 5(a) indicates that Mo-doping can obviously suppress the recombination rate of e^-/h^+ pairs, which causes a decrease in the intensity of the emission peak at 390 nm. In addition, the intensity of this emission peak varied with Mo concentration. The sample Mo(2%)ZnO calcined at 600 °C exhibited the weakest PL peak. However, higher Mo concentrations resulted in an increase in the intensity of the PL peak. Figure 5(b) shows the effects of varying the calcination temperature on the PL emission spectra of Mo(2%)ZnO. It is observed that the samples calcined at low or very high temperatures show strong and sharp emission peaks at around 390 nm. At low calcination temperatures, the poor crystallinity of ZnO could produce more recombination centers for photogenerated electrons and holes, which increases the intensity of the emission peak. However, calcination at very high temperatures may cause the displacement of O^{2-} and Zn^{2+} and produce more O^{2-} or Zn^{2+} vacancies in the ZnO crystal lattice. These vacancies also could become recombination centers for photogenerated electrons and holes. As for the emission peak in the visible light range, increasing temperature only slightly increases

the intensity of this emission peak.

3.6 Photocatalytic performance tests

The photocatalytic activities of the pure ZnO and Mo-doped composites were evaluated by measuring the degradation of acid orange II in aqueous solution under UV light irradiation (λ = 365 nm). From Figure 6(a), it can be seen that acid orange II is only slightly degraded under UV light irradiation without any catalyst, indicating that direct photolysis of acid orange II can be ignored. After 5 h of light irradiation, the degradation ratios of acid orange II over ZnO, Mo(1%)ZnO, Mo(2%)ZnO, Mo(3%)ZnO and Mo(8%)ZnO reached 31.45, 33.27, 62.84, 48.96 and 23.95%, respectively, as shown in Figure 6(b). The increase in Mo concentration from 0 to 2 wt.% effectively promotes the dye degradation rate. However, a further increase in Mo content has an adverse effect. The optimal doping concentration of Mo was found to be 2 wt.%. In addition, the photocatalytic activity of ZnO doped with 2 wt.% Mo depends on the calcination temperature. From Figure 7, it can be seen that the degradation ratios of acid orange II were 51.49, 54.07, 62.84, 56.95 and 45.21% for the Mo(2%)ZnO samples calcined at 400, 500, 600, 700, and 800 °C, respectively. The sample calcined at 600 °C gives the best photocatalytic activity, which is mainly due to the recombination of photogenerated electrons and holes being suppressed by the improvement in crystallinity. However, very high calcination temperatures (700 and 800 °C) decrease the activity, which is mainly caused by the decrease in surface area, increase in crystallite size, and decrease in sample dispersion. To quantitatively understand the reaction kinetics of the acid orange II degradation in our experiments, we used a pseudo-first order model expressed by the equation: $\ln (C_0/C) = kt$, which can be generally used for photocatalytic degradation if the initial concentration of the pollutant is low [32]. C_0 and C are the concentrations of dye in the solution at time 0 and t, respectively, and k is the pseudo-first-order rate constant. The rate constants obtained from the regression of plots of $\ln(C/C_0)$ vs. t are shown in Table 4. A good correlation with pseudo-first order reaction kinetics ($R^2 > 0.96$) was found. The highest reaction rate constant was 0.192 h^{-1} for the sample calcined at 600 °C with 2 wt.% Mo. One problem associated with ZnO in photocatalytic reactions is its photo-instability due to the problem of photocorrosion. The effects of Mo-doping on photostability were investigated by reusing the catalysts. The results are shown in Figure 8. After being used four times, the degradation ratio for ZnO calcined at 600 °C decreased from 28.16 to 9.32%. However, for Mo(2%)ZnO calcined at 600 °C, there was almost no change in degradation ratio. According to the literature [12, 21], the photostability properties of ZnO are strongly dependent on its surface atomic structure. A high surface energy can cause instability of ZnO because this kind of surface is more readily attacked by photogenerated holes. The doping of Mo changes the surface atomic structure of ZnO, which might decrease its surface energy, thus resulting in an increase in photostability.

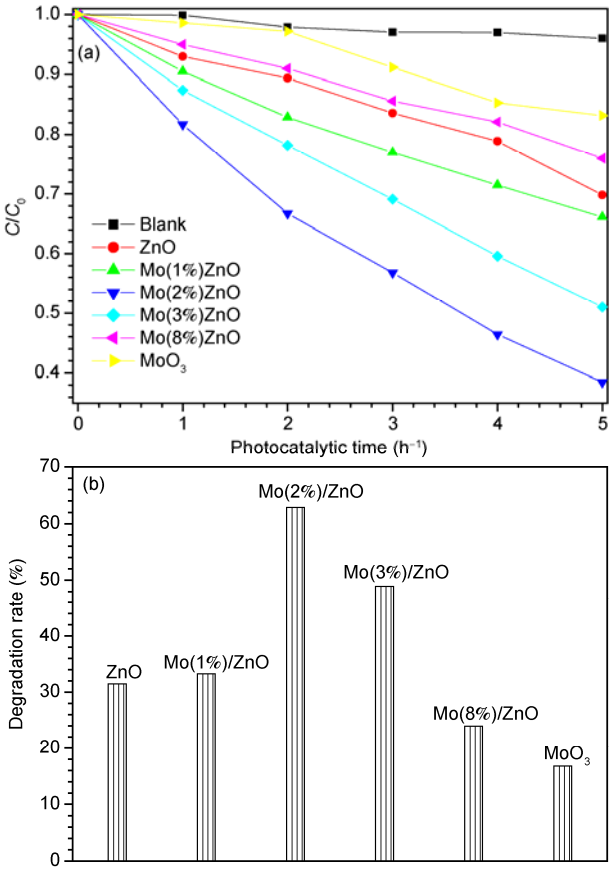

Figure 6 Comparison of the photocatalytic activity of the catalysts with different Mo contents. (a) Changes in dye concentration as a function of irradiation time; (b) the degradation rate of the dye after 5 h irradiation.

Table 4 First-order reaction rate constants of the catalysts in the degradation of acid orange II

Sample	Calcination temperature (°C)	K (h^{-1})	R^2
ZnO	600	0.065	0.98
Mo(1%)ZnO	600	0.085	0.99
Mo(2%)ZnO	600	0.192	0.99
Mo(3%)ZnO	600	0.127	0.99
Mo(8%)ZnO	600	0.051	0.99
Mo(2%)ZnO	400	0.169	0.99
Mo(2%)ZnO	500	0.192	0.99
Mo(2%)ZnO	700	0.173	0.99
Mo(2%)ZnO	800	0.145	0.99

Moreover, the undoped Mo species may exist in the form of MoO_3. Therefore, another possible reason for the high photocatalytic activity over Mo(2%)ZnO could be due to the formation of MoO_3/ZnO heterojunctions as has been reported [33, 34] for the TiO_2/MO_3 system. Therefore, the valence band (VB) edge positions of MoO_3 and ZnO were

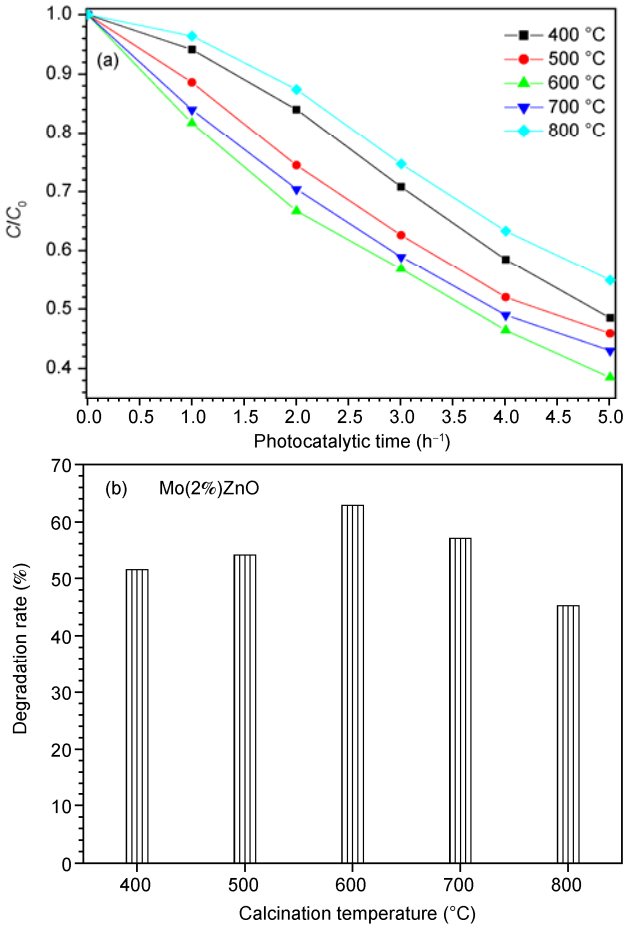

Figure 7 Comparison of the photocatalytic performance of Mo(2%)ZnO calcined at different temperatures. (a) Changes in dye concentration as a function of irradiation time; (b) the degradation rate of the dye after 5 h irradiation.

estimated according to the concept of electronegativity [35, 36]. The conduction band (CB) and VB potentials of the two semiconductors at the point of zero charge can be calculated by the following equation:

$$E_{VB} = X - E^e + 0.5E_g \quad (1)$$

where X is the absolute electronegativity of the semiconductor, which is defined as the geometric mean of the absolute electronegativity of the constituent atoms; E^e is the energy of free electrons on the hydrogen scale (ca. 4.5 eV); E_{VB} is the VB edge potential; and E_g is the band gap of the semiconductor obtained from the equation $E_g = 1240/\lambda_g$ (eV). The CB position can be deduced from the equation $E_{CB} = E_{VB} - E_g$. The X values for MoO_3 and ZnO are ca. 7.2 and 6.0 eV. On the basis of the above equations, the top of the VB and the bottom of the CB of MoO_3 are calculated to be 4.08 and 1.21 eV, respectively. Accordingly, the VB and CB of ZnO are estimated to be 3.10 and –0.09 eV, respectively. According to our estimated E_g values of MoO_3, the CB position of MoO_3 is more anodic than ZnO, and a schematic energy band model of the heterojunction composite can be depicted as shown in Figure 9. Thus, the excited electrons in the CB of ZnO can transfer to the CB of MoO_3. At the same time, holes in the VB of MoO_3 can transfer to the VB of ZnO. Therefore, the MoO_3/ZnO heterojunction could inhibit the recombination of photogenerated carriers, resulting in the enhanced performance of the MoO_3/ZnO composite exhibits as compared to pure ZnO. However, if the MoO_3 content is too high, the dispersion of MoO_3 become poor and the redundant MoO_3 can become recombination centers, resulting in a decrease in photocatalytic activity.

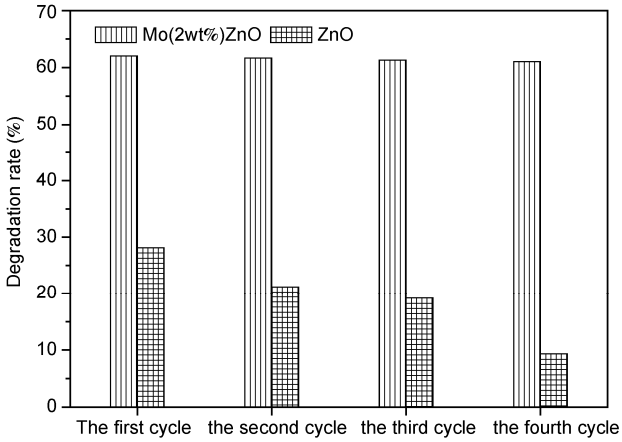

Figure 8 Comparison of the photocatalytic performance of Mo(2%)ZnO and ZnO in the recycled reactions.

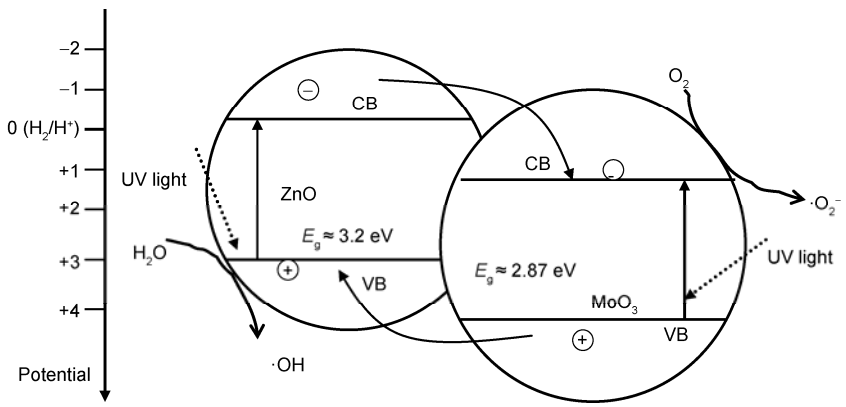

Figure 9 Photocatalytic mechanism of the MoO_3/ZnO composite photocatalyst.

4 Conclusions

The effects of Mo doping on the structural properties of ZnO and its photocatalytic activity in the degradation of acid orange II have been investigated. The addition of Mo can effectively suppress the growth of ZnO particles and enrich the surface hydroxyl groups –OH groups in ZnO. The highest activity and good photostability were observed for Mo(2%)ZnO calcined at 600 °C. The high photocatalytic performance of the Mo-doped ZnO can be attributed to higher level of surface hydroxyl groups, high crystallinity and low recombination rate of electron/hole (e^-/h^+) pairs. The doping of Mo also changes the surface atomic structure of ZnO, which may decrease its surface energy, thus resulting in an increase in photostability.

The project was supported by the National Natural Science Foundation of China (21067004), the Natural Science Foundation of Jiangxi Province, China (2010GZH0048), and Jiangxi Province Educatien Department of Science and Technology Project (GJJ 12344).

1 Jiang YQ, Li FF, Sun R, Xie ZX, Zheng LS. A simple solvothermal route towards the morphological control of ZnO and tuning of its optical and photocatalytic properties. *Sci China Chem*, 2011, 53(8): 1711–1717
2 Yu CL, Yu JC. A simple way to prepare C-N-codoped TiO_2 photocatalyst with visible-light activity. *Catal Lett*, 2009, 129(3-4): 462–470
3 Bui TD, Kimura A, Shigeru I, Matsumura M. Determination of oxygen sources for oxidation of benzene on TiO_2 photocatalysts in aqueous solutions containing molecular oxygen. *J Am Chem Soc*, 2010, 132(24): 8453–8458
4 Yu CL, Yu JC. Sonochemical fabrication, characterization and photocatalytic properties of Ag/$ZnWO_4$ nanorod catalyst. *Mater Sci Eng B*, 2009, 164(1): 16–22
5 Yu CL, Yu JM, Zhou WQ, Yang K. WO_3 coupled P-TiO_2 photocatalysts with mesoporous structure. *Catal Lett*, 2010, 140(3-4): 172–183
6 Hu C, Peng TW, Hu XX, Nie YL, Zhou XF, Qu JH, He H. Plasmon-induced photodegradation of toxic pollutants with Ag–AgI/Al_2O_3 under visible-light irradiation. *J Am Chem Soc*, 2010, 132(2): 857–862
7 Yu CL, Yu JC, Chan M. Sonochemical fabrication of fluorinated mesoporous titanium dioxide microspheres. *J Solid State Chem*, 2009, 182(5): 1061–1069
8 Reynolds DC, Look DC, Jogai B, Hoelscher JE, Sherriff RE, Harris MT, Callahan MJ. Time-resolved photoluminescence lifetime measurements of the Γ_5 and Γ_6 free excitons in ZnO. *J Appl Phys*, 2000, 88(4): 2152–2153
9 Baxter JB, Aydil ES. Dye-sensitized solar cells based on semiconductor morphologies with ZnO nanowires. *Sol Energy Mater Sol Cells*, 2006, 90(5): 607–622
10 Yuhas BD, Yang P. Nanowire-based all-oxide solar cells. *J Am Chem Soc*, 2009, 131(10): 3756–3761
11 Yamazaki T, Wada S, Noma T, Suzuki T. Gas-sensing properties of ultrathin zinc oxide films. *Sens Actuators B*, 1993, 14(1-3): 594-595
12 Chu D, Masuda Y, Ohji T, and Kato K. Formation and photocatalytic application of ZnO nanotubes using aqueous solution. *Langmuir*, 2010, 26(4): 2811–2815
13 Xu J, Chang YG, Zhang YY, Ma SY, Qu Y, Xu CT. Effect of silver ions on the structure of ZnO and photocatalytic performance of Ag/ZnO composites. *Appl Surf Sci*, 2008, 255(5): 1996–1999
14 Wu JJ, Tseng CH. Photocatalytic properties of nc-Au/ZnO nanorod. *Appl Catal B*, 2006, 66(1-2): 51–57
15 Li D, Haneda H. Photocatalysis of sprayed nitrogen-containing Fe_2O_3–ZnO and WO_3–ZnO composite powders in gas-phase acetaldehyde decomposition. *J Photochem Photobiol A*, 2003, 160(3): 203–212
16 Hsu CC, Wu NL. Synthesis and photocatalytic activity of ZnO/ZnO_2 composite. *J Photochem Photobiol A*, 2005, 172(3): 269–274
17 Li D, Haneda H. Synthesis of nitrogen-containing ZnO powders by spray pyrolysis and their visible-light photocatalysis in gas-phase acetaldehyde decomposition. *J Photochem Photobiol A*, 2003, 155(1-3): 171–178
18 Chen LC, Tu YJ, Wang YS, Kan RS, Huang CM. Characterization and photoreactivity of N-, S-, and C-doped ZnO under UV and visible light illumination. *J Photochem Photobiol A*, 2008, 199(2-3): 170–178
19 Hong RY, Qian JZ, Cao JX. Synthesis and characterization of PMMA grafted ZnO nanoparticles. *Powder Technol*, 2006, 163(3): 160–168
20 Hong RY, Chen LL, Li JH, Li HZ, Zheng Y, Ding J. Preparation and application of polystyrene-grafted ZnO nanoparticle. *Polym Adv Technol*, 2007, 18(11): 901–909
21 Kislov N, Lahiri J, Verma H, Goswami DY, Stefanakos E, Batzill M. Photocatalytic degradation of methyl orange over single crystalline ZnO: Orientation dependence of photoactivity and photostability of ZnO. *Langmuir*, 2009, 25(5): 3310–3315
22 Shen YB, Zhou X, Xu M, Ding YC, Duan MY, Linghu RF, Zhu WJ. Electronic structure and optical properties of ZnO doped with transition metals. *Acta Physica Sinica*, 2007, 56(6): 3440–3445
23 Yu CL, Yang K, Yu JC, Peng P, Cao FF, Li X, Zhou XC. Effects of rare earth Ce doping on the structure and photocatalytic performance of ZnO. *Acta Phys-Chim Sin*, 2011, 27(2): 505–512
24 Sanatgar-Delshade E, Habibi-Yangjeh A, Khodadadi-Moghaddam M. Hydrothermal low-temperature preparation and characterization of ZnO nanoparticles supported on natural zeolite as a highly efficient photocatalyst. *Monatsh Chem*, 2011, 142(2): 119–129
25 Roy S, Basu S. Improved zinc oxide film for gas sensor applications. *Bull Mater Sci*, 2002, 25(6): 513–515
26 Jing LQ, Xu ZL, Sun XJ, Shang J, Cai WM. The surface properties and photocatalytic activities of ZnO ultrafine particles. *Appl Surf Sci*, 2001, 180(3-4): 308–314
27 Hufschmidt D, Liu L, Seizer V, Bahnemann D. Photocatalytic water treatment: Fundamental knowledge required for its practical application. *Water Sci Technol*, 2004, 49(4): 135–140
28 Chen YP, Lu CL, Xu L, Ma Y, Hou WH, Zhu JJ. Single-crystalline orthorhombic molybdenum oxide nanobelts: Synthesis and photocatalytic properties. *Cryst Eng Comm*, 2010, 12(11): 3740–3747
29 Wang XH, Zhao DX, Liu YC, Zhang JY, LuYM, Fan XW. The photoluminescence properties of ZnO whiskers. *J Cryst Growth*, 2004, 263(1-4): 316–319
30 Stikant V, Clarke DR. On the optical band gap of zinc oxide. *J Appl Phys*, 1998, 83(10): 5447–5451
31 Meng XQ, Zhao DX, Zhang JY, Shen DZ, Lu YM, Liu YC, Fan XW. Growth temperature controlled shape variety of ZnO nanowires. *Chem Phys Lett*, 2005, 407(1-3): 91–94
32 Yu CL, Fan CF, Yu JM, Zhou WQ, Yang K. Preparation of bismuth oxyiodides and oxides and their photooxidation characteristic under visible/UV-light irradiation. *Mater Res Bull*, 2011, 46(1): 140–146
33 Hirotaka N, Koichi K, Masashi T. Fabrication and photocatalytic activity of TiO_2/MoO_3 particulate films. *J Oleo Sci*, 2009, 58(4): 203–211
34 Yukina T, Pailin N, Tetsu T. Energy storage TiO_2–MoO_3 photocatalysts. *Electrochimica Acta*, 2004, 49(12): 2025–2029
35 Kim Y, Atherton SJ, Brigham E S, Mallouk TE. Sensitized layered metal oxide semiconductor particles for photochemical hydrogen evolution from nonsacrificial electron donors. *J Phys Chem*, 1993, 97: 11802–11810
36 Dai G P, Yu JG, Liu G. Synthesis and enhanced visible-light photoelectron catalytic activity of p–n junction BiOI/TiO_2 nanotube arrays. *J Phys Chem C*, 2011, 115: 7339–7346